3-1998

Diffusivities of n-Alkanes in Silicalite By Steady-State Single-Crystal Membrane Technique

Orhan Talu
Cleveland State University

Matthew S. Sun

Dhananjai B. Shah
Cleveland State University

Publisher's Statement

This is the accepted version of the following article: Talu, O., Sun, M. S. & Shah, D. B. (1998), Diffusivities of n-alkanes in silicalite by steady-state single-crystal membrane technique. AIChE J., 44, 3, 681–694. doi: 10.1002/aic.690440316, which has been published in final form at http://onlinelibrary.wiley.com/doi/10.1002/aic.690440316/abstract

Diffusivities of *n*-Alkanes in Silicalite by Steady-State Single-Crystal Membrane Technique

Orhan Talu, Matthew S. Sun, and D. B. Shah
Dept. of Chemical Engineering, Cleveland State University, Cleveland, OH 44115

A novel experimental technique that measures the diffusive flux through a single-crystal membrane (SCM) was developed and tested. Unlike all other macroscopic techniques that depend on a transient response, SCM is used under steady-state conditions, which results in a wide range of applicability from 10^{-2} to 10^{-11} cm^2/s. Phenomenological equations for the steady-state data analysis were developed. The variation of driving force over the diffusion path is included in the model. As required by thermodynamics, the micropore concentration is given as a function of surface-excess amount adsorbed and gas density. The membrane configuration measures diffusivity in only one crystallographic direction. The micropore diffusivities of C_1 to C_{10} normal alkanes through silicalite crystal in the z-direction were measured at 30, 50 and 70°C. The activation energies for micropore diffusion are also reported. The data agree excellently with the other two studies that measure directional diffusivities. Diffusion and adsorption of hexane and heptane in silicalite display structural heterogeneity induced by the comparable lengths of molecules and silicalite channels rather than diameter of molecule vis-à-vis pore diameter.

Introduction

Adsorption is increasingly gaining industrial importance as new adsorbent materials are introduced and existing systems are optimized (Sircar, 1992). Applications of adsorption cover a wide range of processes from bulk gas separations (oxygen from air, hydrogen production, etc.) to purification, including many environmental applications. In addition, physical adsorption and desorption are the first and last steps of any catalytic reaction. As in any other process, equilibrium and kinetics are the two fundamental aspects that control adsorption. Adsorption equilibrium has become well formalized, starting with J. W. Gibbs (1928). There are several articles that provide the thermodynamic framework of adsorption equilibria (van Ness, 1969; Sircar and Myers, 1973; Myers and Prausnitz, 1965; Talu and Zwiebel, 1986; Sircar, 1985). Although prediction of multicomponent equilibria from pure component adsorption remains a major challenge in adsorption thermodynamics, the systems can be experimentally measured and carefully collected data measured by different techniques, and research groups have been found to be consistent (Valenzuela and Myers, 1989; Talu et al., 1996a,b).

In contrast to adsorption equilibria, kinetic data (diffusivities) reported in the literature exhibit vast differences, reaching several orders of magnitude for some systems. In a series of monographs, Kärger and Ruthven (1989, 1992) have provided an excellent summary of these differences and offer several possible explanations. Being a dynamic property, measurement of diffusivities is inevitably more complicated than measurement of equilibria. Other transport mechanisms, particularly heat transfer, can interfere with the measurements that necessitate careful experimental design and execution to minimize extraneous transfer effects. Calculation of diffusivities from raw data usually involves some kind of a mathematical model with its inherent assumptions and uncertainties. Differences in adsorbent samples, synthesis procedures, and measurement techniques, especially activation/regeneration protocols, are just a few of the possible sources for the inconsistencies in reported diffusivity values. Furthermore, most literature data are sporadic, covering a narrow range in system properties and in the nature of the

diffusant species. Lack of systematic data also hinders the development of plausible explanations for the differences reported in the literature.

In an attempt to explain and consolidate the fragmented knowledge on micropore diffusion, we have been systematically studying the diffusion of *n*-alkane series in silicalite using the single-crystal membrane (SCM) technique. The diffusivity of methane to butane using the transient SCM method was reported earlier (Sun et al., 1996a). The SCM technique is further developed to enable the measurement of micropore diffusivities under steady-state conditions. Here, the diffusivities of *n*-alkanes from methane to decane are reported along with the phenomenological equations necessary for data analysis. To the best of our knowledge, this represents the first successful attempt at measuring micropore diffusivities by a macroscopic method under steady-state conditions. Recently, Lewis et al. (1997) have reported results with a similar technique. They fabricated membranes with a single oriented crystal of ferrierite, measured the permeation rates through the crystal, and determined the diffusivity at steady state. In principle, the two methods are essentially identical except for one significant difference. Our experimental setup is capable of monitoring the transient response as well, whereas theirs is not. Therefore, in our case, we can calculate diffusivity from both transient and steady-state measurements for at least the linear systems. All other macroscopic methods determine diffusivities from a transient response. A short review of diffusion measurement techniques is provided next in order to put the steady-state SCM technique into proper perspective.

Micropore Diffusivity Measurement Techniques

Micropore diffusivity measurement techniques can be grouped into two general categories, depending on the scale of observations: macroscopic and microscopic. A third approach is based on computer simulations, which is not an experimental measurement; yet, they provide important insight into the molecular motion in the micropores for a postulated molecular model.

Macroscopic methods

Macroscopic methods involve measurement of an aggregate property such as pressure, temperature, or concentration. Well-known macroscopic techniques are uptake (gravimetric, Ruthven, 1984; piezometric, Caro et al., 1993), frequency response (FR) (Shen and Rees, 1994; Bourdin et al., 1996), gas chromatographic method (Shah and Ruthven, 1977; Hufton and Danner, 1991), including the zero-length-column (ZLC) (Ruthven et al., 1992), and the isotope-exchange method (Quig and Rees, 1976; Rynders et al., 1997). Most of these methods introduce a disturbance to the system and the diffusivity is deduced from how fast the system approaches new equilibrium conditions; these are all transient methods. Macroscopic methods thus measure transport diffusivities under an imposed concentration gradient. The transport diffusivities are converted into corrected diffusivities using the Darken's correction factor. The fastest diffusivity that can be measured by macroscopic methods is restricted by the response time of measurement devices. Most approaches are limited to diffusivities below 10^{-6}–10^{-7} cm^2/s.

Since most macroscopic methods are based on transient experiments, other transport phenomena such as heat and mass transfer can play a detrimental role. Adsorption is an exothermic process. Earlier diffusivity measurements were plagued by heat-transfer restrictions, as pointed out by Bülow et al. (1984). More recent techniques, such as FR, ZLC, and membrane methods can reduce heat effects to a negligible extent in carefully designed experiments. In fact, a novel approach (Bourdin et al., 1996) is based on the heat effect and the temperature variation it causes. Conceptually, it is not possible to completely eliminate the heat effect since in most cases, the equilibrium is distributed. One way to cause a measurable change without disturbing equilibrium is the use of isotopes, which is the main motivation for the recent techniques based on isotopes (Hufton et al., 1994; Rynders et al., 1997). The heat effects clearly do not exist when isotopes are used. Nevertheless, experiments based on isotopes still use transient measurements, unlike the SCM technique. Analysis of transient data is inevitably more complicated than the steady-state data due to the complexity of the governing equations.

The micro-FTIR (Karge and Niessen, 1991) method can be classified as a macroscopic technique, although it is based on spectroscopic data. The technique measures a transient aggregate property, the rate of change of FTIR signal during adsorption (or desorption) after a step change in gas-phase conditions.

Microscopic methods

Microscopic techniques involve direct measurement of molecular mobility in the pores of an adsorbent under equilibrium conditions. These methods therefore measure self-diffusivities. Microscopic methods include pulsed-field-gradient nuclear-magnetic-resonance (PFGNMR) (Heink et al., 1992), and quasi-elastic-neutron-scattering (QENS) (Jobic et al., 1989). Data analysis is based on relaxation theory applied to molecular mobility. Questions have been raised about the relation between molecular mobility and the Fickian diffusivity especially in a microporous environment (Chen et al., 1994). Nevertheless, the relations seem to hold since the diffusivities measured for some systems with macroscopic and microscopic techniques do agree (Kärger and Ruthven, 1989).

Microscopic methods are especially suitable for fast-diffusing species. The lowest diffusivities these methods can measure are on the order of 10^{-5}–10^{-7} cm^2/s, which is the upper limit for macroscopic techniques. Therefore, the range where both macroscopic and microscopic methods may be used is quite limited. Both approaches are at the limit of their applicability in this range, which has been offered as an explanation for the inconsistencies. Yet, this cannot be true since the two approaches yield comparable results for some systems, while vast unexplained differences exist for some other systems.

Computer simulations

Molecular mobility can also be determined by computer-simulation results by molecular-dynamics (MD) (June et al., 1990) and Brownian-diffusion transition state theory (BD/TST) (Maginn et al., 1996). The diffusivities calculated in computer experiments are dependent on the molecular-

level model postulated for the system. Computer experiments provide molecular mobility and thus the diffusivity for a given molecular model. The model includes representations of the solid structure and the structure of the guest molecules in addition to formulations of all pertinent interactions for solid–gas and gas–gas pairs. This complicated molecular model is usually tested using equilibrium data that may provide some confidence in the parameter values. On the other hand, equilibrium data are based on the measurements of overall system behavior and many different molecular models may result in the same equilibrium behavior. Therefore, molecular simulation results with inherent assumptions in the model can never replace the real phenomena, and these results cannot be used to prove or disprove experimental data. Nevertheless, it is interesting to note that the diffusivity values from simulations, in general, agree with microscopic techniques.

The main power of computer simulations is the clearly linked cause–effect relationships that can be conveniently exploited to compare scenarios that do not even exist in reality. Computer simulations provide a powerful tool to adsorbent developers for screening/directing research to avenues with the highest probability of success for a specific application.

Single-Crystal Membrane Technique

The SCM technique can be classified as a macroscopic method. It is simply based on the direct measurement of diffusion flux through single crystals of zeolite at steady-state conditions. SCM has several advantages over other macroscopic techniques, as detailed in an earlier article about transient measurements for C_1–C_4 *n*-alkanes (Sun et al., 1996a). The transient SCM method depends on time measurements. The fastest diffusivity that can be measured with the transient technique is limited by the response time of the system and is about 10^{-5} cm^2/s. Such an upper limit does not exist for steady-state measurements, as we have been able to measure even Poiseuille flow fluxes through short capillaries. On the other hand, the steady-state method is limited by the sensitivity of the mass-spectroscopic detector and the flow conditions. The estimated lowest diffusivity that can be measured by the steady-state method with the present system is about 10^{-11} cm^2/s. Therefore, the steady-state SCM method covers a wide range of micropore diffusivities. This range also bridges over the limits of both macroscopic and microscopic techniques. Another important advantage of steady-state SCM is the almost complete elimination of heat effects.

At steady state, the mean temperature of the zeolite crystal is equal to the system temperature since the rate of adsorption on one surface is equal to the rate of desorption from the other. On the other hand, a small temperature difference between the two surfaces exists due to adsorption/desorption. The temperature difference causes conductive heat transfer in the solid structure parallel to the diffusion path. The heat-transfer flux is equal to the product of heat of adsorption and diffusion flux. In a typical experiment, the heat of adsorption is about 100 kJ/mol; the diffusive flux is 10^{-7} mol/(cm^2·s) and the length of the crystal is 10^{-2} cm. If the thermal conductivity of the zeolite crystal is assumed equal to that of sand particles (8×10^{-4}) cal/(cm·s·°c), a simple calculation assuming insulated surfaces on the sides of the crystal that are sealed by epoxy indicates that the temperature difference is less than 0.1°C, which is the accuracy of a thermostat bath. The following equation is used for this approximation:

$$J * Q_{st} = k * \frac{\Delta T}{L}. \tag{1}$$

It should be noted that the SCM technique measures directional diffusivity. When the pore system is anisotropic, as with silicalite in this study, the results are not directly comparable to other techniques that measure an effective diffusivity as a combination of diffusion in all directions.

The SCM technique provides transient as well as steady-state data during the same experiment, which may be used as an internal consistency check. Comparison of transient and steady-state results is included in the discussion for systems close to Henry's law behavior, that is, methane to butane in this case. The data-analysis methods for transient data with systems far removed from the Henry's law range are not currently available; therefore, transient data for these systems are excluded from this article.

Experimental System

The heart of the SCM technique is a single zeolite-crystal membrane. In this study, an untwinned (optically checked) silicalite crystal of $100\times100\times300$ μm initial size is embedded in an epoxy with diffusion path parallel to the *z*-axis. Silicalite has a three-dimensional channel network with straight channels aligned in the *y*-direction and zigzag channels parallel to the *x*-*y* plane (Figure 1). The two sides of the membrane were polished and the final crystal size after polishing was $100\times100\times100$ μm. Details of the membrane manufacture are provided elsewhere (Sun et al. 1996a).

The integrity of the membrane was checked by exposure to molecules larger than the silicalite pore diameter of about 5.6 Å. One side of the membrane was exposed to 18-torr pressure of triethyl amine (TEA), which has a critical diameter of 7.4 Å. TEA was not detected on the other side, even after 8 h, indicating structural integrity with the only pathway available between the two sides of the membrane being that through the micropores.

The membrane is placed in a Wicke–Kallenbach-type permeation cell with flow capabilities on both sides, as shown in Figure 2. During the experiments, one side (inlet) is exposed to the diffusing gas, while helium flow is used on the other side (exit) to sweep the diffusant to a high-sensitivity mass-selective detector (MSD). In a typical experiment, the membrane was first activated at 90°C (limited by the possibility of epoxy degradation at higher temperatures), with abundant helium flow on both sides of the membrane at about 1-torr pressure. The helium flow assures that the partial pressure of adsorbate is extremely low. The temperature increase was restricted to 1°C/min to reduce thermal stresses on the membrane. Activation was continued for at least 2 h, although the MSD did not detect any gas other than helium after approximately 30 min. After activation, the membrane was cooled slowly to experimental temperature under reduced helium flow while applying higher vacuum. The helium flow on the

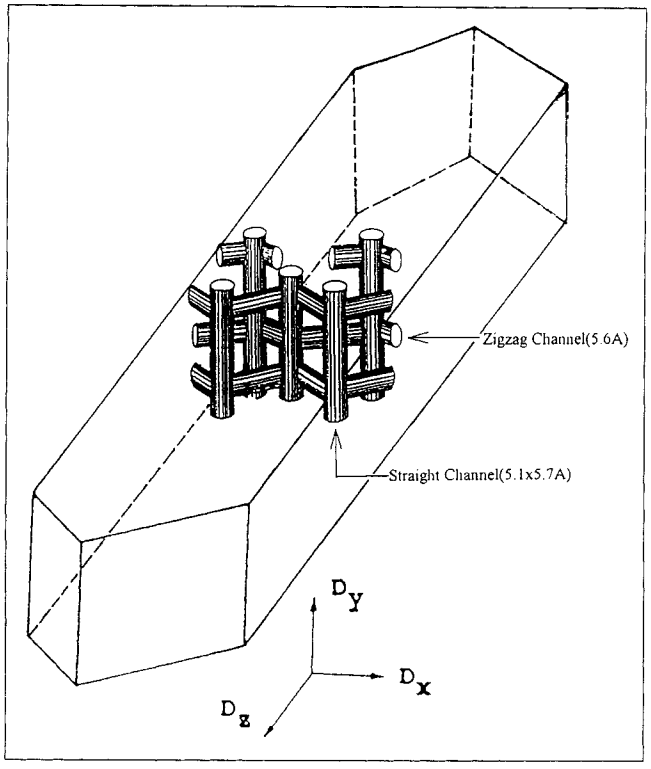

Figure 1. Orientation of the crystal and the associated channel system in silicalite.

exit side was adjusted to 1.5 cm^3 (STP)/min and the entire flow was directed to the MSD. The pressure on the exit side of the crystal membrane was 15 torr during experiments, which was caused by the pressure drop due to helium flow in the custom-made MSD transfer line. The MSD operates at about 10^{-5}-torr pressure. The inlet side was switched to the

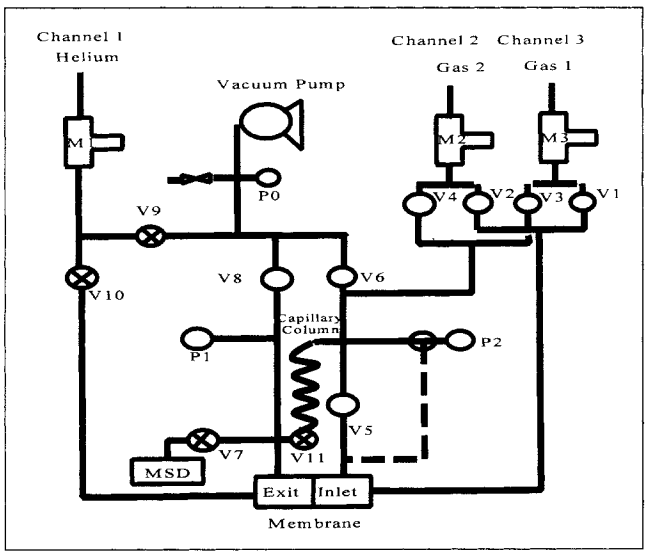

Figure 2. SCM experimental setup.

V1–V5: automatic valves; V6, V8: regulating valves; V7, V9, V10, V11: on/off valves; P0, P1, P2: pressure gauges; M1, M2, M3: mass flow controllers.

diffusant with a small flow of about 10 cc (STP)/min at a pressure of about 10 torr. The MSD response was tracked until it reached steady state, usually within 20 min. The steady-state response level was recorded. This value is converted to diffusion flux using the calibration method described later.

The existence of helium on the exit side and adsorbate on the inlet side would normally correspond to countercurrent diffusion if the system is not selective, such as for polymeric membranes and zeolitic membranes that contain macropores. The only diffusion path in these experiments is through the micropores or by diffusion in the adsorbed phase. Helium is a "nonadsorbing" reference compound used in all adsorption work. Being nonadsorbing, the helium density in micropores equals its gas-phase density of about 0.8 mol/m^3 in these experiments. The density of methane, the alkane with the lowest adsorption, in the micropores is about 25 mol/m^3 or 32 times that of helium. Factoring the molecular weight ratio of 4 since it would affect the collisions of methane and helium molecules in the micropores, the ratio becomes 128. These numbers indicate that helium cannot have any impact on the diffusion of even methane. Similar conclusions were also drawn about the impact of small molecules on the micropore diffusivity of heavier ones by Qureshi and Wei (1990) and Sircar (1992).

As further evidence of membrane integrity and the negligible impact of helium on micropore diffusion, it should be noted that the pressures on the two sides of the membrane were not balanced during these experiments (although the apparatus has such a capability). The exit side of membrane was at a pressure of 15-torr helium and the pressure on the inlet side was between 2 and 10 torr for different species. In fact, the gases were diffusing against a pressure gradient driven by the concentration gradient in the surface phase. Although the pressure differential for helium was 15 torr, it was not observed on the inlet side within the detection limit of the MSD. This is also indisputable evidence that micropore diffusion is the only transport mechanism in the SCM experiments. Such observations are not possible with polymeric membranes, and have yet to be documented for polycrystalline "zeolitic" membranes that have been recently developed (Funke et al., 1996; Baertsch et al., 1996).

Many different membranes were fabricated using different crystals of silicalite grown in the same batch and of similar size and shape. In many cases, identical experiments were performed with different membranes in the diffusion cell. The results reported here were reproducible from membrane to membrane.

MSD response calibration

The diffusive flux in moles per time per cross-sectional area is necessary to calculate the diffusivities from steady-state measurements. The cross-sectional area of the crystals was measured from the scanning electron micrographs of the membrane. The total diffusive flow through the crystals is extremely small, on the order of 10^{-10} moles/s. Although the MSD can detect such low quantities, its response is in arbitrary units of abundance. In addition, the MSD signal usually changes with time and conditions, thereby affecting the accuracy. A calibration protocol utilizing capillary flow was executed after each experiment to circumvent the accuracy prob-

lems. The ions (m/z ratio) with the largest fraction were tracked with the MSD in the experiments.

A capillary tube of 5-m length and 100-micrometer internal diameter was incorporated into the system that connects the inlet and exit sides (Figure 2). The capillary was also housed in the thermostatic bath. After the diffusion measurement was completed, the membrane was isolated and the capillary was opened without disturbing the MSD or the exit-side helium flow. The capillary inlet side pressure was adjusted with the control valve until the MSD response matched the value recorded during the diffusion experiment. The capillary inlet- and exit-side pressures were recorded. Typically, the inlet pressures were in the range of 50–100 torr. Since the pressure on the exit side containing helium was only 15 torr, there was a forced convective flow through the capillary. Laminar compressible flow equations were used to calculate the total flow from the pressure values by the following equation:

$$Q_p = \frac{\pi d^4 (P_1^2 - P_2^2)}{256 L \mu R T}. \tag{2}$$

The flow calculated from Eq. 2 is equal to the diffusive flow through the SCM, since the abundances (MSD response) were matched. Although there is a helium concentration gradient along the capillary, the resulting diffusive flux was negligible compared to the convective flow caused by the relatively high-pressure differential. This complicated calibration technique was adopted because (1) it is performed "on-line" without disturbing the system, (2) it can be used for any gas, circumventing the necessity for numerous standard gases, and (3) it can also be used for binary systems, which is our future goal.

The accuracy of this calibration technique is cross-checked by using standard low-concentration mixtures of butane in helium. The ppm-range of the butane-in-helium mixture was used as the sweep gas. During these tests, the membrane was bypassed and the flow and MSD conditions, and the experimental conditions, were replicated as closely as possible. During these tests, the membrane was bypassed and the flow and MSD conditions, and the experimental conditions, were replicated as closely as possible. Figure 3 shows that the capillary flow calculations (shown as concentration in helium) are in very good agreement with the standard mixtures. The uncertainty introduced by the capillary calibration method is about 5%.

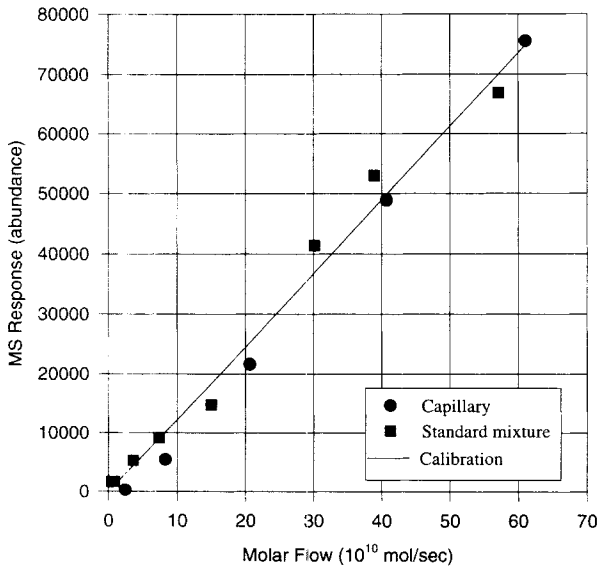

Figure 3. MSD calibration with capillary flow and with standard mixtures.

Corrected Diffusivities from Steady-State Flux

The continuity equation for the diffusant in the zeolite crystal at steady-state conditions is

$$\frac{dJ}{dx} = 0, \tag{3}$$

where J is the diffusion flux and x is the position. Simple integration indicates that the steady-state flux (J_{ss}), is not a function of position in the crystal:

$$J_{ss} \neq f(x). \tag{4}$$

The flux is related to the transport diffusivity, D_t, by Fick's equation:

$$J = -D_t \frac{dq}{dx}, \tag{5}$$

where q is the concentration in the micropores. The transport diffusivity varies with concentration (Karger and Ruthven, 1989). The corrected diffusivity D_0 is defined using a thermodynamic factor called the Darken's correction factor:

$$D_t = D_0 * \frac{d \ln P}{d \ln q} \tag{6}$$

Substitution of Eq. 6 into Eq. 5 yields, after some mathematical manipulation,

$$J = -D_0 q \frac{d \ln P}{dx}. \tag{7}$$

The concentration in this equation refers to moles of gas per volume in the micropores. Thermodynamic definitions provide a link between the concentration and the surface excess amount adsorbed (n), which is the only measurable quantity in adsorption equilibria (Sircar, 1985):

$$q = \rho_{\text{solid}} * n + \epsilon * \rho_{\text{gas}}, \tag{8}$$

where ρ_{solid} is the crystal (particle) density and ϵ is the microporosity. The second term in the summation corrects for the gas density (ρ_{gas}) to obtain the concentration in absolute terms. This correction can be very significant for light gases, as discussed later. At the low-pressure levels in these experiments, the gas density is accurately described by the Ideal Gas law.

$$\rho_{\text{gas}} = \frac{P}{RT}. \tag{9}$$

Table 1. Virial Parameters for *n*-Alkane Adsorption in Silicalite

Carbon No.	a_0	a_1	b_0	b_1	c_0	c_1	d_0	d_1
1	15.2	−2,497.8	0.831	−287.5	0.464	0.000	0.0715	0.000
2	16.9	−3,968.4	0.402	19.85	−0.437	0.000	0.0632	0.000
3	15.7	−4,359.9	3.44	51.38	−5.28	0.000	3.17	0.000
4	15.0	−4,872.3	12.1	−1,115	−16.5	0.000	10.3	0.000
5	15.4	−5,597.2	9.87	−1,691	−7.24	0.000	4.49	0.000
6	25.4	−8,575.2	1.48	0.000	0.0822	0.000	3.61	0.000
7	27.9	−10,180	6.79	0.000	−19.1	0.000	25.0	0.000
8	31.8	−12,040	4.38	0.000	−10.2	0.000	16.3	0.000
9	34.8	−13,646	4.38	0.000	−10.0	0.000	18.5	0.000
10	38.8	−15,600	4.83	0.000	−8.05	0.000	19.2	0.000

P = torr; T = K; N = mol/kg.

Gibbs adsorption isotherm equation at constant temperature relates the spreading pressure (Ψ) to the excess amount adsorbed and the pressure by

$$d\psi = n * d \ln P. \tag{10}$$

The spreading pressure is a primary intensive property of surface phases and can be calculated from isotherm data by integration of the preceding equation.

Combination of above equations gives

$$J_{ss} * dx = -D_0 * \left(\rho_{\text{solid}} * d\psi + \epsilon * \frac{P}{RT} * d \ln P \right). \tag{11}$$

Since J_{ss} is not a function of position, integration of Eq. 11 from inlet to exit gives

$$J_{ss} * L = D_0 \left(\rho_{\text{solid}} * \psi_{\text{inlet}} + \epsilon * \frac{P_{\text{inlet}}}{RT} \right), \tag{12}$$

The total flow (Q) measured in the experiments and the cross-sectional area (A) are used to calculate the flux:

$$J_{ss} = \frac{Q}{A}. \tag{13}$$

Finally, Eqs. 12 and 13 can be rearranged to obtain corrected diffusivity as

$$D_0 = \frac{Q * L}{A \left(\rho_{\text{solid}} * \psi_{\text{inlet}} + \epsilon * \frac{P_{\text{inlet}}}{RT} \right)}. \tag{14}$$

Equation 14 accounts for the variation of concentration along the diffusivity path by formulating the problem in terms of spreading pressure. An implicit assumption made in the above derivation is that D_0 is constant. If surface-phase concentrations are used directly with Eq. 7, an isotherm equation is necessary to relate q to P. The reformulation of the problem in terms of spreading pressure provides a convenient and generic approach to analyze steady-state diffusion data. It also provides an intuitive insight showing that spreading pressure drives the portion of diffusive flow in the surface excess part and pressure drives the correction term.

Pure component isotherms are necessary to calculate the ψ_{inlet} via integration of Eq. 10 unless the experimental conditions correspond to Henry's law behavior. In that case, ψ_{inlet} is equal to the excess amount adsorbed. In this study, the equilibrium data were taken from Abdul-Rehman et al. (1990) for methane to butane, and from Sun et al. (1996b) for pentane to decane. A Virial isotherm equation (Talu et al., 1996a) was curve-fitted to the data in the relevant experimental range to facilitate the integration of Eq. 10:

$$P = N * \exp\left[\left(a_0 + \frac{a_1}{T} \right) + \left(b_0 + \frac{b_1}{T} \right) * N + \left(c_0 + \frac{c_1}{T} \right) * N^2 + \left(d_0 + \frac{d_1}{T} \right) * N^3 \cdots \right]. \tag{15}$$

Due to the complexity of equilibrium behavior of some *n*-alkanes (Sun et al., 1996b), Eq. 15 was curve-fitted to limited low-pressure isotherm data up to experimental pressure levels. Table 1 lists the virial parameter values used in this study.

Results and Discussion

The diffusivities of *n*-alkane series from methane to decane were measured at 30, 50, and 70°C temperature. The corrected diffusivities calculated by Eq. 14 are listed in Table 2. The table also includes the inlet pressure values and the corresponding spreading pressure calculated by the virial isotherm equation. The inlet pressures with higher alkanes were limited by the vapor pressure at ambient conditions.

Corrected diffusivities

The corrected diffusivities are shown against chain length in Figure 4. An immediately apparent feature in the figure is the unexpected increases in diffusivity from hexane to heptane to octane. Normally, the diffusivity is expected to decrease with the chain length. This unusual phenomenon is attributed to the density and location of the molecules in the silicalite pore system. The equilibrium data from pentane to decane have been reported in an earlier article (Sun et al., 1996b). The isotherms of hexane and heptane showed subtle but detectable steps where the second derivatives changed sign (figures 3 and 4 in Sun et al., 1996b). The zero-coverage heats of adsorption for these two compounds also stood out

Table 2. Corrected Diffusivities of *n*-Alkanes in the *z*-Direction in Silicalite

Alkane	T, °C	P, torr	q, mol/m^3	D, cm^2/s
Methane	30	8.66	14.95	3.19×10^{-5}
	50	8.87	9.24	4.15×10^{-5}
	70	9.13	6.11	5.26×10^{-5}
Ethane	30	9.84	363.56	1.13×10^{-5}
	50	10.16	173.25	1.35×10^{-5}
	70	10.69	90.85	1.46×10^{-5}
Propane	30	5.91	1,095.3	2.79×10^{-6}
	50	6.17	591.4	3.85×10^{-6}
	70	6.34	342.1	4.05×10^{-6}
Butane	30	5.94	1,935.1	1.07×10^{-7}
	50	6.12	1,642.9	1.20×10^{-7}
	70	6.32	1,038.9	1.22×10^{-7}
Pentane	30	3.36	2,487.1	1.06×10^{-7}
	50	4.2	2,193.8	1.03×10^{-7}
	70	3.80	1,819.6	7.97×10^{-8}
Hexane	30	3.31	1,644.7	3.02×10^{-8}
	50	4.31	1,390.3	4.22×10^{-8}
	70	3.06	953.5	5.41×10^{-8}
Heptane	30	4.92	1,536.8	4.26×10^{-8}
	50	5.06	1,399.0	7.26×10^{-8}
	70	5.05	1,237.2	9.92×10^{-8}
Octane	30	3.1	1,720.0	2.45×10^{-7}
	50	3.23	1,562.1	2.93×10^{-7}
	70	2.68	1,363.6	4.29×10^{-7}
Nonane	30	3.05	1,728.7	9.17×10^{-8}
	50	3.03	1,580.9	1.41×10^{-7}
	70	3.0	1,419.2	1.85×10^{-7}
Decane	30	1.74	1,687.7	4.55×10^{-8}
	50	5.5	1,537.7	6.00×10^{-8}
	70	1.95	1,378.1	7.50×10^{-8}

of the trend established by other alkanes (see Figure 5). Based on Sun et al. (1996b) data, the highest CH_2 group density is reached with heptane in silicalite pores, with hexane showing slightly lower values. Figure 6 shows a remarkable drop in CH_2 group density in the pores from heptane to octane. A lower packing density can enable higher mobility of the molecules. This unusual equilibrium behavior was attributed to the comparable sizes of hexane and heptane with the length of pores of silicalite, especially the zigzag channels that are about 10 Å long from intersection to intersection. A zigzag channel can be occupied by a single stretched hexane molecule or by a heptane molecule in a spiral configuration.

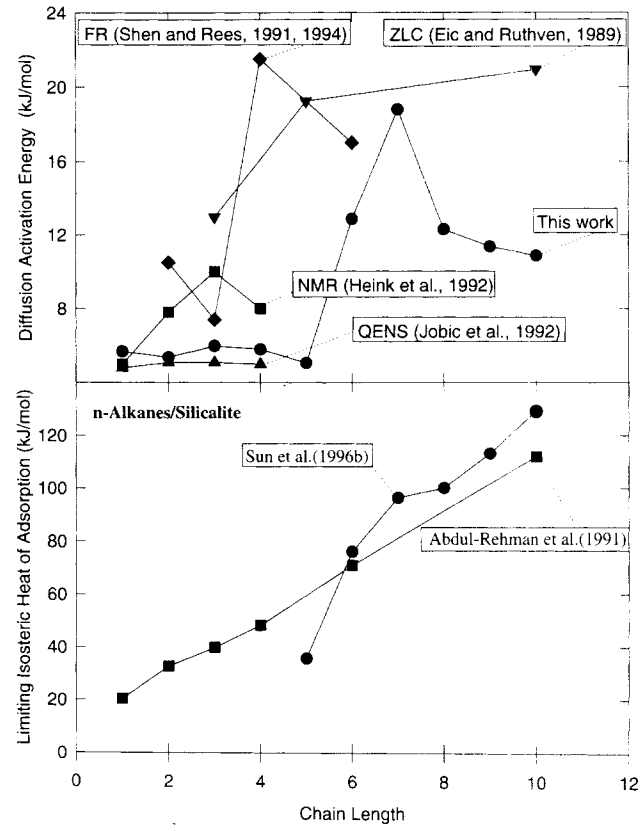

Figure 5. Limiting heat of adsorption and diffusional activation energy of *n*-alkanes in silicalite.

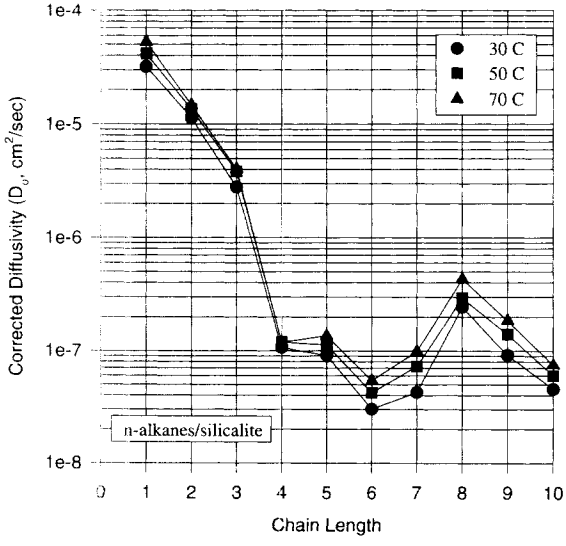

Figure 4. Corrected diffusivities from SCM steady-state measurements for *n*-alkanes in silicalite.

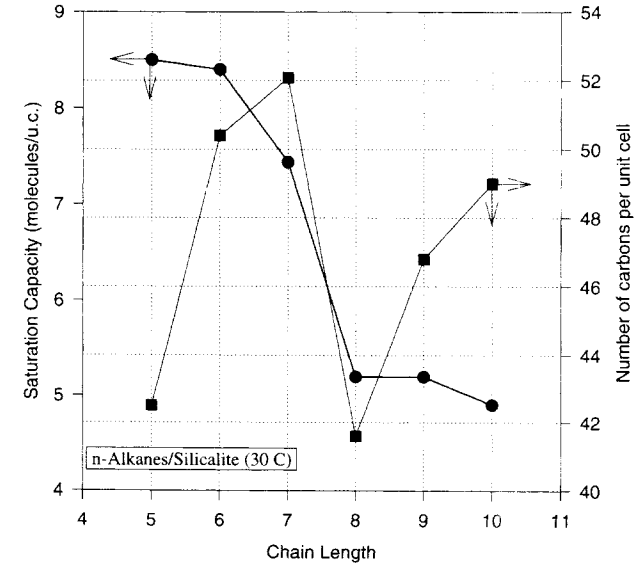

Figure 6. Saturation capacity of *n*-alkanes in silicalite.

There is other recent evidence in the literature about the unusual adsorption behavior of hexane and heptane in silicalite. Temperature-programmed desorption studies by Olson and Reischman (1996) and by van Well et al. (1995) show two distinct extremes in the profile indicating two different environments where hexane is adsorbed. Similarly, unusual equilibrium data were also reported by Richards and Rees (1987). Molecular simulation results by Smit and Siepmann (1994) indicate "freezing" of hexane in the zigzag channels at half-saturation capacity. The diffusion path in the z-direction in our experiments forces the molecules to travel through zigzag and straight channels in sequence (see Figure 1). The diffusion will be retarded if the hexane is "frozen" in the zigzag channels, which acts like a bottleneck.

Longer alkanes do not fit in a single channel. Although heptane and octane molecules are long enough to occupy two straight segments in sequence, such a configuration does not contribute to the diffusion flux. Hence, they must occupy both types of channels simultaneously. The leading CH_2 groups in a chain that may be in a straight channel can act like a guide for the remainder of the chain in a zigzag channel for a smoother move between the two channels. This scenario coupled with the lower CH_2 density in the system explains the substantial increase in diffusivity from heptane to octane in Figure 4.

Activation energy for diffusion

Figure 7 shows the diffusivities as a function of temperature. The slopes of lines in Figure 7 are the diffusion activation energies that are listed in Table 3 along with the limiting

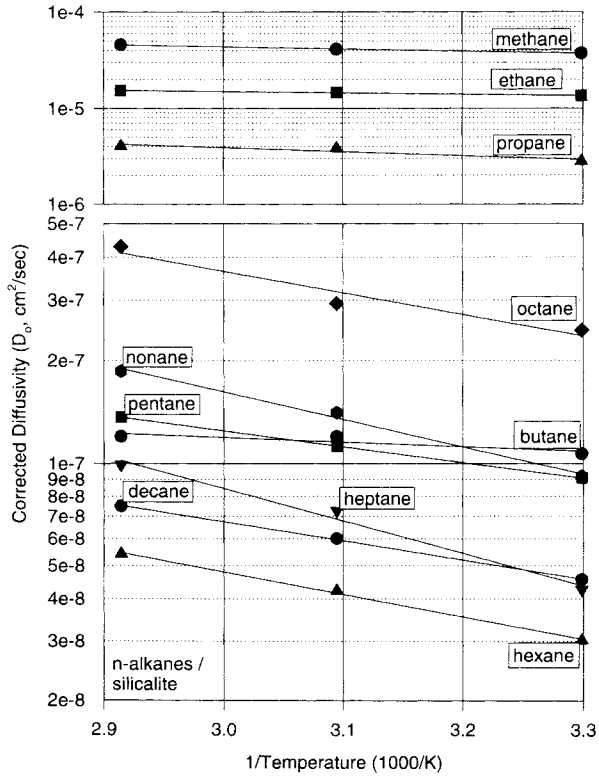

Figure 7. Effect of temperature on diffusivity of *n*-alkanes in silicalite.

Table 3. Heat of Adsorption and Diffusional Activation Energy for *n*-Alkanes in Silicalite

Carbon No.	ΔH_{ad}, kJ/mol	E, kJ/mol
1	20.39*	5.69
2	32.78*	5.38
3	39.85*	6.00
4	48.27*	5.81
5	35.80**	5.06
6	76.18**	12.86
7	96.40**	18.78
8	100.1**	12.30
9	113.2**	11.36
10	129.4**	10.86

*Abdul-Rehman et al. (1990).
**Sun et al. (1996a).

heats of adsorption (from Sun et al., 1996b). Figure 5 shows both activation energy and the heat of adsorption as a function of chain length. In general, potential barriers related to activation energies are much smaller than those related to the heats of adsorption. The activation energy is about 5.5 kJ/mol and does not change significantly from methane to pentane, in agreement with the QENS results of Jobic et al. (1992a,b). The activation energies by PFGNMR (Heink et al., 1992) and ZLC (Eic and Ruthven, 1989) show mixed trends. At this point, it should be emphasized that our results are for directional diffusivity in the z-direction, while others are for a combined effective diffusivity. The activation energy measured in our experiments increase substantially after pentane, reaching 19 kJ/mol for heptane, which is almost four times higher than that for pentane. The activation energy decreases from octane to decane. These trends are in complete agreement with the previous stipulations about the unusual equilibrium and diffusion behavior of hexane and heptane.

Behavior of n-alkanes in silicalite channels

The results presented here in combination with equilibrium data suggest three distinct regimes of adsorption and diffusion of n-alkanes in silicalite according to chain length: (1) methane to propane (C_1–C_3); (2) butane to heptane (C_4–C_7); and (3) octane to decane (C_8–C_{10}).

The C_1–C_3 molecules are small enough so that two or more molecules can fit in a channel lengthwise. The isotherms are all type I and the limiting heats of adsorption at zero coverage increase linearly with carbon number. Also, the isosteric heat of adsorption increases linearly with coverage (Sun et al., 1996b). The diffusivity drops monotonically and the diffusion activation energy is almost constant with respect to chain length. These are indications of a relatively homogeneous system.

The C_4–C_7 molecules are large enough to exclude the possibility of two molecules in the same channel, yet small enough to be contained completely in a single channel segment. This causes a substantial drop in diffusivity in comparison to C_1–C_3. There is a significant void space in the channels for butane and pentane, as indicated by the CH_2 densities. The limiting heats of adsorption and activation energies for butane and pentane are in line with those for C_1–C_3, while hexane and heptane stand out of the trend with respect to both the limiting heats and activation energies. Hexane has the lowest diffusivity (even lower than decane) since its

size almost exactly matches the length of the zigzag channels. These are indications of a heterogeneous system. Heterogeneous behavior is induced for C_4–C_7 due to the comparable lengths of the molecules and the channels.

The behavior of the C_8–C_{10} group is similar to that of the C_1–C_3 group in several respects. Isotherms are type I, although they are extremely steep. The heat of adsorption increases linearly with carbon number and the diffusivity drops montonically. The diffusion activation energies show a small decreasing trend but well within the experimental uncertainty. However, there is an important difference. C_8–C_{10} molecules are longer than the length of the channels and hence simultaneously occupy both channels in contrast to multiple molecules occupying the same channel simultaneously for C_1–C_3. Nevertheless, the C_8–C_{10} adsorption in silicalite reverts back to homogenous behavior similar to that exhibited by C_1–C_3 systems.

Silicalite does not contain aluminum. Thus cations do not exist in the structure. Observations of heterogeneous behavior can only be attributed to structural effects related to the dimensions of the pores. Structural heterogeneity of silicalite adsorption systems caused by comparable diameters of aromatic molecules and pores was reported earlier (Talu et al., 1989; Guo et al., 1989; Li and Talu, 1993). Heterogeneous behavior in adsorption induced by the comparable length of guest molecules and channels has never been as clearly demonstrated as described earlier for C_6–C_7 in silicalite based on equilibrium and kinetic data.

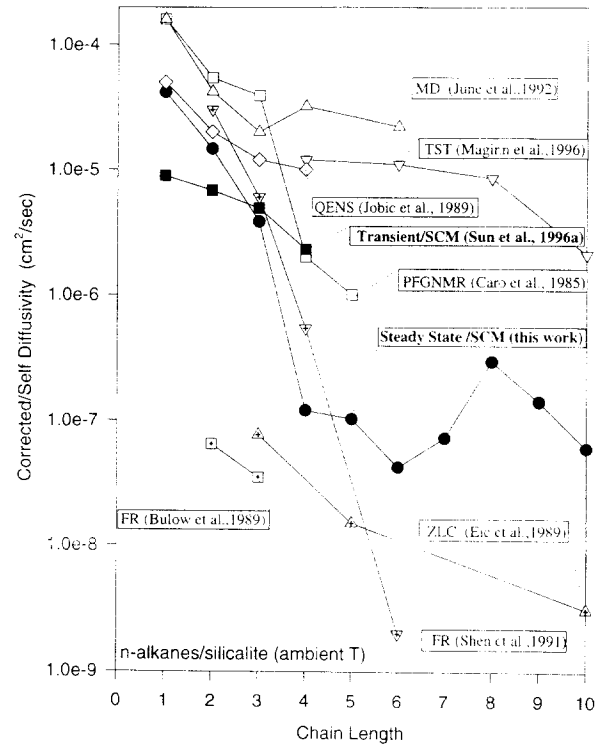

Figure 8. Comparison of diffusivities of *n*-alkanes in silicalite from different techniques.

Comparison of diffusivities with literature data

Figure 8 shows a compilation of literature data on the diffusivity of *n*-alkanes in silicalite along with our results. Several points need to be emphasized here. The diffusivities from microscopic techniques are self-diffusivities determined under the conditions of equilibrium. The diffusivities determined from macroscopic techniques are transport diffusivities that have been converted into corrected diffusivities. Since self-diffusivities are equal to corrected diffusivities only near zero loading, we have tried as much as possible to include the corrected diffusivities at or near zero loadings from the cited references. Our own data on the figure are subject to the limitation imposed by the assumption that D_0 is independent of loading.

The figure is quite crowded, but it clearly demonstrates some of the reasons for the concerns about the inconsistencies in diffusivity values in the literature. For example, the MD result by June et al. (1990) for hexane (2×10^{-5} cm^2/s) is almost 10,000 times larger (four orders of magnitude) than the FR measurements by Shen and Rees (1994). Some literature data are not even included in the figure since it was not possible to fit all on a reasonable scale (Chiang et al., 1984; Hufton and Danner, 1991). Table 4 lists all diffusion data for these systems that we were able to find in the literature.

A closer examination of the data in Figure 8 and their sources establishes a few trends. In general, the results of microscopic techniques, such as PFGNMR (Heink et al., 1992) and QENS (Jobic et al., 1992a,b), are higher than those of macroscopic methods such as FR (Shen and Rees, 1994) and ZLC (Ruthven et al., 1992). Computer simulation results, such as MD (June et al., 1992) and BD/TST (Maginn et al., 1996), fall closer to the microscopic methods. From methane to propane, PFGNMR, QENS, MD, and BD/TST results are all in good agreement at approximately 10^{-5} cm^2/s. On the other hand, two macroscopic techniques, FR by Bülow et al. (1989) and ZLC by Eic and Ruthven (1989) are in agreement with each other at about 10^{-8} cm^2/s. The difference between the two groups is an astonishing three orders of magnitude.

For C_4 and C_5 alkanes, the results of microscopic methods also start diverging from each other with more than an order of magnitude difference; MD at 2×10^{-5}, QENS and BD/TST at 10^{-5}, and PFGNMR at 10^{-6} cm^2/s. Macroscopic ZLC measurements, on the other hand, show 10^{-8} cm^2/s, or two orders of magnitude lower than the lowest microscopic measurement. The data are sporadic for higher alkanes, but the differences seem to persist. An interesting case in Figure 8 is the FR data by Shen and Rees (1991, 1994), which seem to agree with microscopic methods for lower alkanes, but dropping several orders of magnitude for hexane (even lower then ZLC results).

Can these differences be explained by the different methods being applicable at different ranges and the data presented in Figure 8 being obtained at the limit of accuracy of each technique? Such an explanation has been suggested by Kärger and Ruthven (1989). Or, is there a fundamental difference between what is measured by macroscopic and microscopic techniques? Macroscopic methods measure "diffusivity" while there are gradients in the system. Microscopic methods measure "mobility" without any gradients in the system. If there is a fundamental difference, why do the data for certain systems agree between macroscopic and microscopic techniques (Kärger and Ruthven, 1981, 1989)? Or, are the discrepancies displayed in Figure 8 simply due to the nature of pentasil zeolites? Silicalite has been shown to display

Table 4. Self-Corrected Diffusivity Data Reported in the Literature for *n*-Alkanes in Silicalite

T, K	Method	D_0, cm^2/s	E, kJ/mol	Reference
Methane				
300	MD	1.6×10^{-4}	5.6	June et al. (1990)
300	MD	1.34×10^{-4}		Goodbody et al. (1991)
300	NMR	1.6×10^{-4}	5.0	Caro et al. (1985)
300	MD	1.6×10^{-4}	4.3	Nicholas et al. (1993)
250	QENS	5.0×10^{-5}	4.8	Jobic et al. (1989)
334	MD	3.6×10^{-5}		Catlow et al. (1991)
300	MBRN	1.1×10^{-6}		Hayhurst and Paravar (1988)
300	CHTGY	1.3×10^{-10}	22	Chiang et al. (1984)
323	SCM*	4.1×10^{-5}	5.7	This work
323	SCM**	8.9×10^{-6}	5.1	Sun et al. (1996a)
Ethane				
299	NMR	5.4×10^{-5}	7.8	Caro et al. (1985)
323	FR	3.0×10^{-5}		Van-Den-Begin et al. (1989)
300	QENS	2.0×10^{-5}		Jobic et al. (1992b)
298	FR	1.3×10^{-5}	10.5	Van-Den-Begin et al. (1989)
334	MBRN	2.2×10^{-7}		Hayhurst and Paravar (1988)
298	FR	6.5×10^{-8}	21.3	Bülow et al. (1989)
298	CHTGY	3.1×10^{-8}	7.8	Hufton and Danner (1991)
323	SCM*	1.5×10^{-5}	5.3	This work
323	SCM**	6.8×10^{-6}	4.8	Sun et al. (1996a)
Propane				
313	NMR	3.9×10^{-5}	1.0	Caro et al. (1985)
300	MD	2.0×10^{-5}		Nicholas et al. (1993)
300	QENS	1.2×10^{-5}	5.1	Jobic et al. (1992b)
323	FR	6.0×10^{-6}		Van-Den-Begin et al. (1989)
333	FR	5.0×10^{-6}	7.4	Van-Den-Begin et al. (1989)
303	ZLC	7.7×10^{-8}	12.97	Eic and Ruthven (1989)
334	MBRN	7.3×10^{-8}		Hayhurst and Paravar (1988)
298	FR	3.5×10^{-8}	20.4	Bülow et al. (1989)
400	CHTGY	2.9×10^{-11}	45.0	Chiang et al. (1984)
323	SCM*	3.8×10^{-6}	6.0	This work
323	SCM**	4.9×10^{-6}	8.1	Sun et al. (1996a)
Butane				
300	MD	3.2×10^{-5}	5.0	June et al. (1992)
300	MD	1.7×10^{-5}		Goodbody et al. (1991)
300	QENS	1.0×10^{-5}	5.0	Jobic et al. (1992a)
300	NMR	2.0×10^{-6}	8.0	Datema et al. (1991)
323	FR	5.4×10^{-7}	21.5	Van-Den-Begin et al. (1989)
297	MBRN	5.7×10^{-8}	19.6	Paravar and Hayhurst (1984)
300	BD/TST	1.2×10^{-5}	5.68	Maginn et al. (1996)
323	SCM*	1.2×10^{-7}	5.8	This work
323	SCM**	2.3×10^{-6}	9.9	Sun et al. (1996a)
Pentane				
300	NMR	1.0×10^{-6}		Datema et al. (1991)
323	ZLC	1.5×10^{-8}	19.24	Eic and Ruthven (1989)
323	SCM*	1.0×10^{-7}	5.1	This work

Table continued

*Steady-state SCM.
**Transient SCM.
Note: CHTGY = chromatography; MBRN = membrane.

Table 4. Self-Corrected Diffusivity Data Reported in the Literature for *n*-Alkanes in Silicalite (Continued)

T, K	Method	D_0, cm^2/s	E, kJ/mol	Reference
Hexane				
300	MD	2.2×10^{-5}		June et al. (1992)
373	QENS	6.9×10^{-6}		Jobic et al. (1992a)
323	UPTK	3.0×10^{-9}		Bülow et al. (1989)
325	FR	2.0×10^{-9}	17	Van-Den-Begin et al. (1989)
300	BD/TST	1.1×10^{-5}	4.7	Maginn et al. (1996)
323	SCM*	4.2×10^{-8}	12.9	This work
Heptane				
323	SCM*	7.2×10^{-8}	18.8	This work
Octane				
300	BD/TST	8.5×10^{-6}	4.3	Maginn et al. (1996)
323	SCM*	2.9×10^{-7}	12.3	This work
Nonane				
323	SCM*	1.4×10^{-7}	11.4	This work
Decane				
373	ZLC	3.1×10^{-9}	20.92	Eic and Ruthven (1989)
300	BD/TST	2.1×10^{-6}	11.2	Maginn et al. (1996)
323	SCM	6.0×10^{-8}	10.9	This work
$C_{12}H_{26}$				
300	BD/TST	1.9×10^{-6}	11.6	Maginn et al. (1996)
$C_{14}H_{30}$				
343	ZLC	2.3×10^{-9}	19.25	Eic and Ruthven (1989)
300	BD/TST	1.3×10^{-6}	13.1	Maginn et al. (1996)
$C_{16}H_{34}$				
300	BD/TST	1.1×10^{-6}	11.3	Maginn et al. (1996)
$C_{20}H_{42}$				
343	ZLC	2.0×10^{-9}	18.83	Eic and Ruthven (1989)
300	BD/TST	7.8×10^{-7}	13.4	Maginn et al. (1996)

*Steady-state SCM.
**Transient SCM.
Note: CHTGY = chromatography; MBRN = membrane.

numerous unusual equilibrium behavior; solid phase transformations induced by loading of gas molecules (Van Koningsveld et al., 1989), steps on adsorption isotherms of aromatics (Talu et al., 1989), steps in binary adsorption isotherms of aromatics at constant pressure (Li and Talu, 1993), recent findings about the steps in hexane and heptane isotherms elaborated earlier (Sun et al., 1996b), etc. A rational and consistent explanation of wide discrepancies displayed in Figure 8 eludes us. In this respect, our frustration is similar to that experienced by many other researchers before us.

Bearing in mind that this study reports directional diffusivities in the z-direction only and other data in Figure 8 are for overall effective diffusivity, the steady-state SCM results are in good agreement with microscopic techniques for lower alkanes up to propane. The diffusivities are closer to results by other macroscopic techniques for higher alkanes. The entire diffusivity range displayed in Figure 8 is within the range of accuracy of the steady-state SCM method.

The diffusivity data for methane to butane by transient SCM (Sun et al., 1996a) are also shown in Figure 8. There are differences between transient and steady-state results. As stipulated in the original article, methane and ethane diffusivities are too fast to be measured by the transient method as their diffusional time constants approach the system time lag. On the other hand, propane and butane deviate from Henry's law behavior, which renders the constant diffusivity assumption in the transient analysis model somewhat questionable. The Fick's second law of diffusion needs to be solved with diffusivity as a function of coverage. This shortcoming of transient measurements was a major motivating factor to develop the steady-state SCM technique reported herein.

Comparison of directional diffusivities

The silicalite pore system is anisotropic as shown in Figure 1. The straight channels with 5.7×5.1-Å cross section are parallel to the y-direction. The zigzag channels in the x-y plane of about 5.6-Å diameter interconnect successive layers

of straight channels. The critical diameter of *n*-alkanes is smaller than both channel diameters but large enough to prevent overlapping of molecules. The CH_2 groups can only overlap in the intersections, which are irregularly shaped, with about 10 Å as the longest free distance. Although the channel diameters are close to each other and larger than the critical diameter of alkanes, the anisotropy causes significantly different diffusivities in different directions.

The differences in directional diffusivities are easily determined from computer simulations. The experimental technique used in this study clearly measures the directional diffusivity in the *z*-direction. There are two other experimental studies in the literature that report directional diffusivity. Hong et al. (1991) were able to align zeolite crystals in capillary tubes that were then loaded in the PFGNMR apparatus. By directing the magnetic field parallel and perpendicular to the capillaries, they were able to measure diffusivities in the *z*-direction, D_z, and in the *x*-*y* plane, *Dxy*. In another study, Caro et al. (1993) were able to orient zeolite crystals in an electrical field. After orientation, selective surfaces of the crystals were coated with an impermable substance to prevent the molecules from entering the pore system in that direction. They measured the diffusivity by the traditional uptake method in the *z*-direction and in the $x - y$ plane using coated crystals.

The directional diffusivity results by these techniques for methane are listed in Table 5. The table also contains an average diffusivity in the $x - y$ plane and the ratio of that to D_z. Although there are differences reported by different research groups, the differences are much smaller than discrepancies displayed in Figure 8. Diffusion in the *y*-direction is fastest due to the large straight channels, while diffusion in the *z*-direction is slowest since the molecules have to travel through straight and zigzag channels in sequence. The ratio of D_{xy} to D_z varies between 4.5 and 8.1. A theoretical approach given by Kärger (1991) predicts the value of the ratio as 5.0. The D_z value listed in Table 5 in the present study at 4×10^{-5} cm^2/s is about twice that obtained from the PFGNMR results and compares well with the BD/TST results by Maginn et al. (1996).

Most macroscopic measurements yield an overall effective diffusivity, *D*. The effective diffusivity is not a simple average of the directional diffusivities, as aspect ratio of the crystals used in experiments has an important effect on the results. Consider an uptake measurement where all surfaces of a single crystal are exposed to the diffusant. The experiment basically measures weight increase transient caused by diffusion in all directions into the crystal or the total flow rate into the crystal. The flow rate through each surface, on the other hand, is a multiplication of the flux with the cross-sectional area in that direction. Therefore, the aspect ratio that determines the relative magnitudes of cross-sectional areas plays an important role in determining the value of the total flow. Pentasil zeolites typically have aspect ratios of 1:1:3 in the *x*:*y*:*z* directions. Therefore, the normal area to diffusion in the *y*-direction (which is equal to that in the *x*-direction) is three times larger than the normal area in the *z*-direction. From Table 5, the D_y calculated in molecular simulations are 5 to 12.5 times larger than D_z. Therefore, a rough estimate of the relative contribution of D_y to macroscopically measured overall diffusivity is in the range 15 to 37.5 times that of D_z. When diffusion in the *x*-direction is also factored in the final result, the *z*-direction contribution to the overall diffusion measurements becomes even smaller. This was experimentally shown by Caro et al. (1993), who measured the overall diffusivity for methane in ZSM-5 as 4.5×10^{-9} m^2/s at 250 K and the $x - y$ component of diffusivities at 300 K as 7.2×10^{-9} m^2/s. Considering the temperature difference, these values indicate that the overall diffusivity is almost completely determined by the $x - y$ components.

Figure 9 shows our results (which are basically D_z) in comparison to the literature diffusivity data from different sources in the *z*-direction. The figure shows a much better agreement between different data sets than that displayed in Figure 8. One set of data in the figure originates from computer simulations. The two experimental data points on the figure in addition to our extensive set are for (1) methane by PFGNMR (Hong et al., 1991) at 1.6×10^{-5} (300 K) compared to our result of 4×10^{-5} cm^2/s (303 K), and (2) *n*-hexane by uptake with coated crystals (Caro et al., 1993) at 8×10^{-8} (298 K) compared to our result of 4×10^{-8} cm^2/s (303 K). Considering the large differences in diffusivity values reported in the literature, the agreement of *z*-direction diffusivities by the steady-state SCM method reported in this study with microscopic PFGNMR and macroscopic uptake measurements is remarkable.

Effect of gas density correction on surface excess amount adsorbed and diffusivity

The only experimentally measurable property depicting the extent of adsorption is the surface excess amount adsorbed as shown so eloquently by Sircar (1985, 1996). The surface excess amount adsorbed (commonly and erroneously referred to in the literature as the amount adsorbed) was introduced

Table 5. Diffusivity in the *z*-Direction for Methane in Silicalite Reported in the Literature

Method	Temp. K	D_x	D_y	D_z	D_{xy}	D_{xy}/D_z	Reference
MD	400	27.0	31.6	6.3	29.3	4.65	June et al. (1990)
MD	298	3.6	14.9	1.2	9.25	7.71	Demontis et al. (1992)
MD	300	6.5	14	1.5	10.3	6.87	Nicholas et al. (1993)
MD	298	13.4	23.8	3.0	18.6	6.2	Goodbody et al. (1991)
MD	298	4.4	13.3	1.1	8.85	8.1	Nowak et al. (1991)
MD	300	16	27.4	5.1	21.7	4.25	Maginn et al. (1993)
PFGNMR	298			1.6	7.2	4.5	Hong et al. (1991)
SCM*	303			5.2			This work
SCM**	303			0.82			Sun et al. (1996a)

Note: $D_{xy} = (D_x + D_y)/2$; $D = (D_x + D_y + D_z)/3$; Multiplier = 10^{-5} cm^2/s.
*Steady-state SCM.
**Transient SCM.

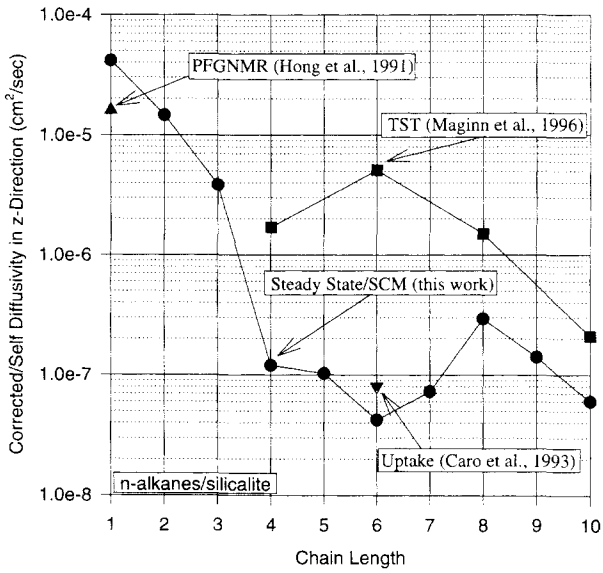

Figure 9. Diffusivities of *n*-alkanes in the *z*-direction in silicalite.

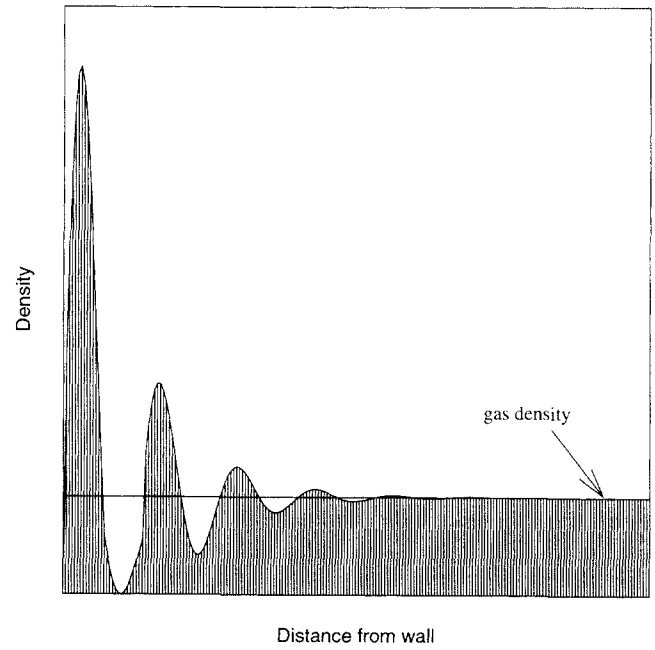

Figure 10. Density profile close to the surface.
From Segura and Chapman, 1995.

by J.W. Gibbs to make adsorption thermodynamics tractable. It is a thermodynamic property accounting for the higher density of a surface phase compared to the adjoining fluid phase. Figure 10 shows density profiles near a flat surface from a molecular simulation (Segura and Chapman, 1995). The details of the simulation are immaterial for the present purpose of explaining the surface excess amount adsorbed. The surface excess amount adsorbed is defined as an integral of the difference of actual density minus the fluid density over the "interfacial region" regardless of whether the surface is flat or the adsorption occurs in micropores

$$n = \text{Area} * \int_0 (\rho_{\text{actual}}(z) - \rho_{\text{gas}})\, dz. \qquad (16)$$

The integrand in Eq. 16 fluctuates between positive and negative values, as depicted in Figure 10. The integrand vanishes at a distance sufficiently far away from the surface where the actual density becomes equal to the fluid density. On the other hand, this "sufficient" distance changes with conditions extending further into the fluid phase as overall density increases. The region where the solid influences the fluid-phase properties is ill-defined. That was the reason for the introduction of surface excess amount adsorbed by J. W. Gibbs. The thermodynamic framework of adsorption equilibria is based on the surface excess amount adsorbed, which circumvents the ill-defined problem. Location of the solid "wall" in microporous solids is not as clear as shown in Figure 10. This problem is experimentally circumvented by measuring the "void space" where low-pressure helium molecules can penetrate. The solid volume is calculated by subtracting the void space from the total volume. Helium is assumed to be "nonadsorbing," implying that helium density at low pressure in the immediate vicinity of a solid equals its gas density.

In adsorption kinetics, the absolute concentration in the micropores appears in the flux expression (see Eq. 7). From thermodynamics, the absolute concentration comprises two parts corresponding to the surface excess amount adsorbed and the fluid phase density as shown in Eq. 8. It is a common and erroneous practice in the diffusion literature to neglect the contribution by the fluid-phase density. The ratio of micropore diffusivity with and without the gas-phase density correction would be infinity for helium since it is nonadsorbing. In fact, neglecting the gas contribution results in a physically impossible picture if helium is the diffusant. Consider an experiment where a zeolite membrane is exposed to a differential helium pressure. If the gas contribution in Eq. 8 is neglected, there would not be any flux going through that membrane, since the surface excess amount adsorbed for helium is zero by definition. In reality, helium would diffuse (and quite rapidly) given the pressure differential.

Conclusions

A new experimental technique for measuring micropore diffusivities based on direct measurement of steady-state flux through a single zeolite crystal in a membrane arrangement has been developed. The technique, named SCM, is the only macroscopic method that measures directional diffusivity at steady-state conditions in contrast to others that measure an overall diffusivity from a transient response. The data analysis is shown to be much simpler under steady-state conditions. The slowest diffusivity that can be measured by SCM is 10^{-11} cm^2/s and there is no upper limit. Therefore, the SCM method covers the entire range of micropore diffusivities overlapping the ranges of both microscopic and macroscopic experiments.

The SCM technique is applied to *n*-alkanes from methane to decane diffusing in silicalite. Adsorption and diffusion behavior of the *n*-alkanes–silicalite system changes from relatively homogeneous to heterogeneous and back to near homogeneous nature as the chain length increases from 1 to 10.

Hexane and heptane show unusual hetergeneous behavior and is attributed to structural heterogeneity caused by the comparable lengths of molecules and pores.

The directional diffusivity results by SCM in the z-direction are in excellent agreement with the results of two other experimental efforts devoted to measuring directional diffusivity. It is clearly shown that the overall diffusivities measured by other techniques are not directly comparable to directional diffusivity. Directional diffusivity values reported here can be instrumental in testing molecular simulations that can differentiate between diffusivities in different directions.

By rigorous application of thermodynamics, it is shown that the inclusion of gas-phase density with the surface excess amount adsorbed is important in expressing the concentration in the micropores in the diffusion equations. This is especially true for nonadsorbing or weakly adsorbed species. The relative contribution from the gas-phase term decreases with increasing adsorption strength for higher hydrocarbons.

The SCM technique opens many new research avenues. The wide range of applicability was the main motivation in developing the technique. The range of SCM encompasses the range of both microscopic techniques (PFGNMR and QENS) and macroscopic techniques (uptake, FR, ZLC, etc.). Similar to many researchers in the past, our data do not offer a plausible explanation for the vast differences in diffusivity values reported in the literature by different research groups. More systematic experiments, possibly including multicomponent systems, are necessary in order to resolve the well-documented problems in the diffusivity data.

Acknowledgments

The authors gratefully acknowledge financial support from the National Science Foundation (CTS-9313661) and Air Products and Chemicals, Inc.

Notation

$a_0, a_1, b_0, b_1,$
c_0, c_1, d_0, d_1 = virial isotherm equation constants
d = capillary diameter, m
k = thermal conductivity, w/m/K
L = diffusion path length, m
N = amount adsorbed, mol/kg
P = pressure, torr
Q_p = flow through the capillary tube, mol/s
Q_{st} = isosteric heat of adsorption, kJ/mol
t = time, s
R = gas constant
T = temperature, °C or K
μ = viscosity of gas, kg/(m·s)
Δ = change in property

Subscripts

1,2 = inlet and exit, respectively

Literature Cited

Abdul-Rehman, H. B., M. A. Hasanain, and K. F. Loughlin, "Quaternary, Ternary, Binary and Pure Component Sorption on Zeolites: 1. Light Alkanes on Linde S-115 Silicalite at Moderate to High Pressures," *Ind. Eng. Chem. Res.*, **29**, 1525 (1990).

Baertsch, C. D., H. H. Funke, J. L. Falconer, and R. D. Noble, "Permeation of Aromatic Hydrocarbon Vapors through Silicalite—Zeolite Membranes," *J. Phys. Chem.*, **100**, 7676 (1996).

Bourdin, V., A. Germnus, P. Grenier, and J. Kärger, "Application of the Thermal Frequency Response Method and of PFGNMR to Study Water Diffusion in Zeolite NaX," *Adsorption*, **2**, 205 (1996).

Bülow, M., P. Struve, and W. Mietk, "Experimental Evidence of the Influence of Sorption-Heat Release Process on the Sorption Kinetics of Benzene in NaX Zeolite Crystals," *J. Chem. Soc., Faraday Trans.*, **80**(1), 813 (1984).

Bülow, M., H. Schlodder, L. V. C. Rees, and R. E. Richards, "Molecular Mobility of Hydrocarbon ZSM/Silicalite System Studied by Sorption Uptake and FR Methods," *Proc. Int. Conf. on Zeolites*, Amsterdam, Netherlands, p. 579 (1989).

Caro, J., M. Bülow, W. Schirmer, J. Kärger, W. Heink, and H. Pfeifer, "Microdynamics of Methane, Ethane, and Propane in ZSM-5 Type Zeolites," *J. Chem. Soc., Farad. Trans.*, **81**, 2541 (1985).

Caro, J., M. Noack, J. Richter-Mendau, F. Marlow, D. Petersohn, M. Griepentrog, and J. Kornatowski, "Selective Sorption Uptake Kinetics of n-Hexane on ZSM-5—A New Method for Measuring Anisotropic Diffusivities," *J. Phys. Chem.*, **97**, 13685 (1993).

Catlow, C. R. A., C. M. Freeman, B. Vessal, S. M. Tomlinson, and M. Leslie, "Molecular Dynamics Studies of Hydrocarbon Diffusion in Zeolites," *J. Chem. Soc., Faraday. Trans.*, **87**, 1947 (1991).

Chen, N. Y., T. F. Degnam, Jr., and C. M. Smith, "Molecular Transport and Reaction in Zeolites: Design and Application of Shape Selective Catalysts," VCH (1994).

Chiang, A. S. T., A. G. Dixon, and Y. H. Ma, "The Determination of Zeolite Crystal Diffusivity by GC: II. Experimental," *Chem. Eng. Sci.*, **39**, 1461 (1984).

Datema, K. P., C. J. J. den Ouden, W. D. Yista, P. C. E. Kuipers, M. F. M. Post, and J. Kärger, "Fourier-Transform Pulsed-Field-Gradient ^{1}H Nuclear Magnetic Resonance Investigation of the Diffusion of Light n-Alkanes in Zeolite ZSM-5," *J. Chem. Soc., Farad. Trans.*, **87**, 1935 (1991).

Demontis, P., G. B. Suffritti, E. S. Fois, and S. Quartieri, "Molecular Dynamics Study on Zeolites. 6. Temperature Dependence of Diffusion of Methane in Silicalite," *J. Phys. Chem.*, **96**, 1482 (1992).

Eic, M., and D. M. Ruthven, "Intracrystalline Diffusion of Linear Paraffins and Benzene in Silicalite Studied by the ZLC Method," *Proc. Int. Conf. on Zeolites*, Elsevier, Amsterdam, p. 897 (1989).

Funke, H. H., M. G. Kovalchick, J. L. Falconer, and R. D. Noble, "Separation of Hydrocarbon Isomer Vapors with Silicalite Zeolite," *Ind. Eng. Chem. Res.*, **35**, 1575 (1996).

Gibbs, J. W., Collected Works, Yale Univ. Press, New Haven, CT (1928).

Goodbody, S. J., K. Watanabe, D. M. Gowan, J. P. R. B. Walton, and N. Quirke, "Molecular Simulation of Methane and Butane in Silicalite," *J. Chem. Soc., Farad. Trans.*, **87**(13), 1951 (1991).

Guo, C.-J., O. Talu, and D. T. Hayhurst, "Phase Transition and Structural Heterogeneity: Benzene Adsorption on Silicalite," *AIChE J.*, **35**, 573 (1989).

Hayhurst, D. T., and A. R. Paravar, "Diffusion of C_1 to C_5 Normal Paraffins in Silicalite," *Zeolites*, **8**, 27 (1988).

Heink, W., J. Kärger, and H. Pfeifer, "High-Temperature Pulsed Field Gradient Nuclear Magnetic Resonance Self-diffusion Measurement of n-Alkanes in MFI-type Zeolites," *J. Chem. Soc., Farad. Trans.*, **88**(23), 3505 (1992).

Hong, U., J. Kärger, R. Kramer, H. Pfeifer, and G. Seiffert, "PFG NMR Study of Diffusion Anisotropy in Oriented ZSM-5 Type Zeolite Crystallites," *Zeolites*, **11**, 816 (1991).

Hufton, J. R., and R. P. Danner, "Gas-Solid Diffusion and Equilibrium Parameters by Tracer Pulse Chromatography," *Chem. Eng. Sci.*, **46**, 2079 (1991).

Hufton, J. R., S. Brandani, and D. M. Ruthven, "Measurement of Intracrystalline Diffusion by Zero Length Column Tracer Exchange," *Zeolites and Related Microporous Materials*, J. Weitkamp, H. G. Karge, H. Pfeifer, and W. Holderich, eds, Elsevier, Amsterdam, p. 1321 (1994).

Jobic, H., M. Bee, J. Caro, M. Bülow, and J. Kärger, "Molecular Self-Diffusion of Methane in Zeolite ZSM-5 by Quasi-Elastic Neutron Scattering and Nuclear Magnetic Resonance Pulsed Field Gradient Technique," *J. Chem. Soc., Farad. Trans.*, **85**(1), 4201 (1989).

Jobic, H., M. Bee, and J. Caro, "Translational Mobility of n-Butane and n-Hexane in ZSM-5 Measured by Quasi-Elastic Neutron Scattering," *Proc. Int. Conf. on Zeolites*, Montreal, Canada, p. 121 (1992a).

Jobic, H., M. Bee, and G. L. Kearley, "Dynamics of Ethane and Propane in Zeolite ZSM-5 Studied by QENS," *Zeolites*, **12**, 146 (1992b).
June, R. L., A. T. Bell, and D. N. Theodorou, "Molecular Dynamics Studies of Butane and Hexane in Silicalite," *J. Phys. Chem.*, **94**, 8232 (1990).
June, R. L., A. T. Bell, and D. N. Theodorou, "Molecular Dynamics Study of Butane and Hexane in Silicalite," *J. Phys. Chem.*, **96**, 1051 (1992).
Karge, H. G., and W. Niessen, "A New Method for the Study of Diffusion and Counter Diffusion in Zeolites," *Catal. Today*, **8**, 451 (1991).
Kärger, J., and D. M. Ruthven, "Diffusion in Zeolites: Comparison of Sorption and NMR Diffusivities," *J. Chem. Soc., Farad. Trans.*, **77**, 1485 (1981).
Kärger, J., and D. M. Ruthven, "On the Comparison Between Macroscopic and NMR Measurements of Intracrystalline Diffusion in Zeolites," *Zeolites*, **9**, 267 (1989).
Kärger, J., "Random Walk Through Two-Dimensional Networks: A Simple Means to Correlate the Coefficients of Anisotropic Diffusion in ZSM-5 Type Zeolites," *J. Phys. Chem.*, **95**, 5558 (1991).
Kärger, J., and D. M. Ruthven, *Diffusion in Zeolites and Other Microporous Solids*, Wiley, New York (1992).
Lewis, J. E., G. R. Gavalas, and M. E. Davis, "Permeation Studies on Oriented Single-Crystal Ferrierite Membranes," *AIChE J.*, **43**, 83 (1997).
Li, J., and O. Talu, "Structural Effect on Molecular Simulations of Tight-Pore Systems," *J. Chem. Soc., Farad. Trans.*, **89**, 1683 (1993).
Maginn, E. J., A. T. Bell, and D. N. Theodorou, "Transport Diffusivity of Methane in Silicalite from Equilibrium and Nonequilibrium Simulations," *J. Phys. Chem.*, **97**, 4173 (1993).
Maginn, E. J., A. T. Bell, and D. N. Theodorou, "Dynamics of Long *n*-Alkanes in Silicalite: A Hierarchical Simulation Approach," *J. Phys. Chem.*, **100**, 7155 (1996).
Myers, A. L., and J. M. Prausnitz, "Thermodynamics of Mixed-Gas Adsorption," *AIChE J.*, **11**(1), 121 (1965).
Nicholas, J. B., F. R. Trouw, J. E. Mertz, L. E. Iton, and A. J. Hopfinger, "Molecular Dynamics Simulation of Propane and Methane in Silicalite," *J. Phys. Chem.*, **97**, 4149 (1993).
Nowak, A. K., C. J. J. den Ouden, S. D. Pickett, B. Smit, A. K. Cheetham, M. F. M. Post, and J. M. Thomas, "Mobility of Adsorbed Species in Zeolites: Methane, Ethane and Propane Diffusivities," *J. Phys. Chem.*, **95**, 848 (1991).
Olson, D. H., and R. T. Reischman, "Structure Related Paraffin Sorption in ZSM-5," *Zeolites*, **17**, 434 (1996).
Paravar, A. R., and D. T. Hayhurst, "Direct Measurement of Diffusivity for Butane Across a Single Large Silicalite Crystal," *Proc. Int. Conf. on Zeolites*, Reno, NV, p. 217 (1984).
Quig, A., and L. V. C. Rees, "Self-Diffusion of *n*-Alkanes in Type A Zeolite," *J. Chem. Soc., Farad. Trans.*, **72**, 771 (1976).
Quresh, W. R., and J. Wei, "One- and Two-Component Diffusion in Zeolites ZSM-5," *J. Catal.*, **126**, 126 (1990).
Richards, R. E., and L. V. C. Rees, "Sorption and Packing of *n*-Alkane Molecules in ZSM-5," *Langmuir*, **3**, 335 (1987).
Ruthven, D. M., *Principles of Adsorption and Adsorption Processes*, Wiley, New York (1984).
Ruthven, D. M., P. Stapleton, and K. Dahlke, "Application of the ZLC Method to the Measurement of Intracrystalline Counter-Diffusion in Liquid-Zeolite Systems," *Proc. Int. Conf. on Zeolites*, Montreal, Canada (1992).
Rynders, R., M. Rao, and S. Sircar, "Isotope Exchange Technique for Measurement of Gas Adsorption Equilibria and Kinetics," *AIChE J.*, **43**, 2456 (1997).
Segura, C. J., and W. G. Chapman, "Associating Fluids with Four Bonding Sites Against Solid Surfaces: Monte Carlo Simulations," *Mol. Phys.*, **86**, 415 (1995).
Shah, D. B., and D. M. Ruthven, "Measurement of Zeolites Diffusivities and Equilibrium Isotherm by Chromatography," *AIChE J.*, **23**, 804 (1977).
Shen, D., and L. V. C. Rees, "Adsorption and Diffusion of *n*-Butane and 2-Butyne in Silicalite-1," *Zeolites*, **11**, 684 (1991).
Shen, D., and L. V. C. Rees, "Study of Fast Diffusion in Zeolites Using a Higher Harmonic Frequency Response Method," *J. Chem. Soc., Farad. Trans.*, **90**(19), 3011 (1994).
Sircar, S., and A. L. Myers, "Surface Potential Theory of Multi-Layer Adsorption from Gas Mixtures," *Chem. Eng. Sci.*, **28**, 489 (1973).
Sircar, S., "Excess Properties and Thermodynamics of Multicomponent Adsorption," *J. Chem. Soc., Farad. Trans.*, **81**, 1527 (1985).
Sircar, S., "Novel Application of Adsorption Technology," *Fundamentals of Adsorption*, M. Suzuki, ed., Kodansha, Japan, p. 3 (1992).
Sircar, S., "Data Representation for Binary and Multicomponent Gas Adsorption Equilibria," *Adsorption*, **2**, 327 (1996).
Smit, B., and J. L. Siepmann, "Simulating the Adsorption of Alkanes in Zeolites," *Science*, **264**, 1118 (1994).
Sun, M. S., O. Talu, and D. B. Shah, "Diffusion Measurements Through Embedded Zeolite Crystals," *AIChE J.*, **42**, 3001 (1996a).
Sun, M. S., O. Talu, and D. B. Shah, "Adsorption Equilibrium of C_5–C_{10} Normal Alkanes in Silicalite Crystals," *J. Phys. Chem.*, **100**, 17276 (1996b).
Talu, O., and I. Zwiebel, "Multicomponent Adsorption Equilibria of Non-Ideal Mixtures," *AIChE J.*, **32**(8), 1263 (1986).
Talu, O., C.-J. Guo, and D. T. Hayhurst, "Heterogeneous Adsorption Equilibria with Comparable Molecule and Pore Sizes," *J. Phys. Chem.*, **93**(21), 7294 (1989).
Talu, O., J. Li, R. Kumar, P. Mathias, J. D. Moyer, Jr., and J. M. Schork, "Measurement and Correlation of Oxygen/Nitrogen/ 5A —Zeolite Adsorption Equilibria for Air Separation," *Gas Sep. Purif.*, **10**, 149 (1996a).
Talu, O., "Equilibrium Measurement Techniques for Screening New Adsorbent Materials," *Proc. World Cong. of Chem. Eng.*, San Diego, CA (1996b).
Valenzuela, D. P., and A. L. Myers, *Adsorption Equilibrium Data Handbook*, Prentice Hall, Englewood Cliffs, NJ (1989).
Van-Den-Begin, L. V. C. Rees, J. Caro, and M. Bülow, "Fast Adsorption-Desorption Kinetics of Hydrocarbons in Silicalite-1 by the Single Step Frequency Response Method," *Zeolites*, **9**, 287 (1989).
Van Koningsveld, H., F. Tuinstra, H. van Bekkum, and J. C. Jansen, "The Location of *p*-Xylene in a Single Crystal of Zeolite H-ZSM-5 with a New, Sorbate Induced, Orthorhombic Framework Symmetry," *Acta Cryst. B*, **45**, 423 (1989).
Van Ness, H. C., "Adsorption of Gases on Solids," *Ind. Eng. Chem. Fundam.*, **8**(3), 464 (1969).
Van Well, W. J. M., J. P. Wolthuizen, B. Smit, J. H. C. van Hooff, and R. A. van Santen, "Commensurate Freezing of *n*-Alkanes in Silicalite," *Angew. Chem. Int. Ed. Engl.*, **34**(22), 2543 (1995).